Agricultural and Forest Meteorology 186 (2014) 1–11

Contents lists available at ScienceDirect

Agricultural and Forest Meteorology

journal homepage: www.elsevier.com/locate/agrformet

Mapping daily evapotranspiration at field scales over rainfed and irrigated agricultural areas using remote sensing data fusion ☆☆

C. Cammalleri [a,*], M.C. Anderson [a], F. Gao [a], C.R. Hain [b], W.P. Kustas [a]

[a] U.S. Department of Agriculture, Agricultural Research Service, Hydrology and Remote Sensing Laboratory, Beltsville, MD, USA
[b] Earth System Science Interdisciplinary Center, University of Maryland, College Park, MD, USA

ARTICLE INFO

Article history:
Received 10 May 2013
Received in revised form 30 October 2013
Accepted 2 November 2013

Keywords:
Thermal remote sensing
Surface energy balance
Multi-sensor data fusion

ABSTRACT

Continuous monitoring of daily evapotranspiration (ET) at field scale can be achieved by combining thermal infrared remote sensing data information from multiple satellite platforms, given that no single sensor currently exists today with the required spatiotemporal resolution. Here, an integrated approach to field-scale ET mapping is described, combining multi-scale surface energy balance evaluations and a data fusion methodology, namely the Spatial and Temporal Adaptive Reflectance Fusion Model (STARFM), to optimally exploit spatiotemporal characteristics of image datasets collected by the Landsat and Moderate resolution Imaging Spectroradiometer (MODIS) sensors, as well as geostationary platforms. Performance of this methodology is evaluated over adjacent irrigated and rainfed fields, since mixed conditions are the most challenging for data fusion procedures, and in two different climatic regions: a semi-arid site in Bushland, TX and a temperate site in Mead, NE. Daytime-total ET estimates obtained for the Landsat overpass dates suggest that the intrinsic model accuracy is consistent across the different test sites (and on the order of 0.5 mm d^{-1}) when contemporaneous Landsat imagery at 30-m resolution is available. Comparisons between tower observations and daily ET datastreams, reconstructed between overpasses by fusing Landsat and MODIS estimates, provide a means for assessing the strengths and limitations of the fused product. At the Mead site, the model performed similarly for both irrigated and rainfed fields, with an accuracy of about 0.9 mm d^{-1}. This similarity in performance is likely due to the relatively large size of the fields (≈50 ha), suggesting that the soil moisture dynamics of the irrigated fields are reasonably well captured at the 1-km MODIS thermal pixel scale. On the other hand, the accuracy of daily retrievals for irrigated fields at the Bushland site was lower than that for the rainfed field (errors of 1.5 and 1.0 mm d^{-1}, respectively), likely due to the inability of the model to capture ET spikes right after irrigation events for fields substantially smaller than MODIS data resolution. At this site, the irrigated fields were small (≈5 ha) compared to the MODIS pixel size, and sparsely distributed over the landscape, so sporadic contributions to ET from soil evaporation due to irrigation were not captured by the 1-km MODIS ET retrievals. However, due the semiarid environment at Bushland, these irrigation-induced spikes in soil evaporation are not long-lived and these underestimations generally affect the irrigation dates only and they do not seem to influence negatively the estimates at the seasonal scale. ET data fusion is expected to perform better over agricultural areas where irrigation is more spatially continuous, resulting in moisture fluxes that are more uniform at the MODIS pixel scale. Overall, the model accurately reproduces the ET temporal dynamics for all the experimental sites, and is able to capture the main differences that were observed between irrigated and rainfed fields at both daily and seasonal time scales.

☆☆ The U.S. Department of Agriculture (USDA) prohibits discrimination in all its programs and activities on the basis of race, color, national origin, age, disability, and where applicable, sex, marital status, familial status, parental status, religion, sexual orientation, genetic information, political beliefs, reprisal, or because all or part of an individual's income is derived from any public assistance program. (Not all prohibited bases apply to all programs.) Persons with disabilities who require alternative means for communication of program information (Braille, large print, audiotape, etc.) should contact USDA's TARGET Center at +1 202 720 2600 (voice and TDD). To file a complaint of discrimination, write to USDA, Director, Office of Civil Rights, 1400 Independence Avenue, S.W., Washington, DC 20250-9410, or call +1 800 795 3272 (voice) or +1 202 720 6382 (TDD). USDA is an equal opportunity provider and employer.

* Corresponding author at: European Commission, Joint Research Centre, Institute for Environment and Sustainability, TP280 Via E. Fermi 2749, I-21027 Ispra (VA), Italy. Tel.: +39 (0)332 78 9869.
E-mail addresses: cammillino@gmail.com, carmelo.cammalleri@jrc.ec.europa.eu (C. Cammalleri).

0168-1923
http://dx.doi.org/10.1016/j.agrformet.2013.11.001

1. Introduction

Agricultural areas occupy approximately 3,730,000 km^2 (38%) of the total land area in the U.S. (www.agcensus.usda.gov). Of this agricultural land, about 5–7% is routinely irrigated to enhance crop yield and quality (Ozdogan and Gutman, 2008). This small portion generates about 50% of the total amount of agricultural crop income (Schaible and Aillery, 2012). In 2005, 490,000 million m^3 per day of water were used for irrigation, corresponding to 62% of total freshwater withdrawals if thermoelectric power is excluded (http://ga.water.usgs.gov/edu/wuir.html). These statistics highlight the need for accurate monitoring of water use at field scales over large irrigated agricultural areas, such as irrigation districts, to facilitate optimization of water use and allocation among different competing uses.

In the last two decades, major improvements in large-area estimates of actual evapotranspiration (ET) have been obtained through remote sensing methods based on thermal infrared (TIR) data, which have become increasingly available from a variety of satellite systems. The land-surface temperature (LST) derived from these observations plays a key role in the partitioning of available energy between turbulent fluxes of sensible and latent heat, the latter of which describes the land-surface water loss to the atmosphere. As reported in several reviews (e.g., Kalma et al., 2008; Liang et al., 2010), these approaches appear to accurately reproduce ET over a wide range of conditions at both the satellite overpass time and daily time scales. For example, the multi-scale TIR-based ALEXI (Atmosphere-Land EXchange Inverse) model and associated flux disaggregation algorithm, DisALEXI, have been successfully applied across the U.S. (Norman et al., 2003; Anderson et al., 2012a), European Mediterranean regions (Cammalleri et al., 2012), as well as over Africa (Anderson et al., 2012b), using polar orbiting satellites (Landsat series, Moderate resolution Imaging Spectroradiometer – MODIS), geostationary platforms (Geostationary Operational Environmental Satellite – GOES, Meteosat Second Generation – MSG), and airborne datasets.

Despite these significant advances in both remote sensing technologies and environmental modeling, deficiencies in the current suite of thermal satellite data sources (e.g., data gaps, biases, inaccurate calibration, poor spatial or temporal resolution) can strongly limit the applicability of such procedures for continuous monitoring of ET at high spatiotemporal resolution (i.e., daily ET at field scale). The modeling of ET at such detailed temporal and spatial scales requires the ability to capture the principal traits of daily ET, including: (i) long-term (weekly/monthly) trends, primarily dictated by plant growth (changes in leaf area, fraction cover and canopy height) and variation in water availability in the root zone (water stress); (ii) day-to-day fluctuations related to changes in meteorological forcing (i.e., air temperature and humidity, solar radiation); and (iii) sporadic peaks, due to increase in soil evaporation fluxes after rainfall/irrigation events. These ET features are generally observable at different spatial scales: (i) large-scale (several km) dynamics, due to spatial patterns in meteorological forcing; (ii) mid-range (km) patterns, due to changes in water availability caused by rainfall events; and (iii) local (field)-scale variability, due to spatial heterogeneity in crop type and phenological stage as well as localized irrigation applications.

No single TIR satellite system currently operating is capable of capturing all of these features of ET dynamics across agricultural landscapes. Hence, the fusion of multiple data sources (e.g., GOES, MODIS and Landsat) seems a particularly appealing strategy for integrating the best qualities of each dataset within a multi-disciplinary mathematical modeling scheme. Because these different data sources are characterized by a wide range of spectral–temporal–spatial resolution and sensor view angles, a fundamental requirement of the adopted modeling framework must be to ensure consistency among ET estimates obtained from different sources at different scales.

The ET flux fusion methodology applied here is based on daily continental-scale ET estimates obtained from the ALEXI model using hourly thermal data from geostationary satellites at 10-km spatial resolution. Higher spatial resolution ET maps are obtained via the DisALEXI disaggregation procedure using both MODIS (1-km, daily) and Landsat (30-m, 16-day) data. The ET end-product, characterized by both fine spatial resolution and temporal frequency, is obtained by fusing MODIS and Landsat derived ET maps using the Spatial and Temporal Adaptive Reflectance Fusion Model (STARFM). The proposed approach aims at ensuring consistency among the ET maps obtained at different spatial resolutions by using the coarse-scale ALEXI estimates as a common normalization basis, while accounting for local-scale features and day-to-day dynamics by combining information from high spatial resolution Landsat and high temporal frequency MODIS imagery.

The performance of this ET data fusion methodology was demonstrated by Cammalleri et al. (2013) over a rainfed agricultural area in central Iowa, effectively capturing impacts on ET of rainfall events occurring between Landsat overpasses. In this paper, we evaluate the ability of this modeling system to correctly account for irrigation effects on ET fluxes. Over large districts of contiguous irrigated fields, the irrigation applications act like a leveling factor, reducing the variability in crop water availability among fields with the same crop species. This generally helps the data fusion process, which requires the presence of homogenous pixels at both high and coarse resolution. More problematic is the modeling of mixed areas, where sparsely distributed irrigated fields are surrounded by rainfed crops (or by natural vegetation). In this case, the availability of representative wet, coarse resolution pixels is more limited, especially when irrigated fields are significantly smaller than the coarse resolution pixel size. The response to irrigation applications may vary significantly between different soil–plant systems, and between climatic regions. In dry environments, soil response to the applied water is faster than under humid conditions; additionally, advective conditions will further increase the magnitude of ET fluxes from irrigated areas. Finally, the method of irrigation also plays a role in the process; while sprinkler systems generally result in large wetted areas (similar in some respects to rainfall), more parsimonious systems (e.g., drip irrigators, not considered here) substantially reduce the wetted area, and hence the soil evaporation losses.

The goal of this work is to evaluate the performance of this ET data fusion approach for two typical U.S. crops, corn and cotton, grown under different climatic conditions and under rainfed and irrigated management. With this aim, the model was applied at two test sites during the growing season (June–September): a dry environment in Bushland (TX) during 2008 and a humid environment in Mead (NE) in 2003. In these experiments both irrigated and rainfed fields were monitored using flux towers, representing two cases of mixed irrigated/unirrigated landscape. The collection of sites corresponds to a wide combination of management practices and meteorological conditions, which lead to large differences in crop water stress and spatial patterns in evaporative fluxes across the landscape. Hence these sites represent a challenging test of the fusion methodology's ability to accurately quantify the effects of irrigation at daily and seasonal scales in agricultural systems.

2. Methods

2.1. The ALEXI/DisALEXI model

Estimates of surface energy fluxes at the time of satellite overpass over heterogeneous agricultural landscapes can be obtained

using the TIR-based Two-Source Energy Balance (TSEB) model, schematized by Norman et al. (1995) and revised by Kustas and Norman (1999) as:

$$R_{n,s} - G_0 = H_s + \lambda E_s \quad (1)$$

$$R_{n,c} = H_c + \lambda E_c \quad (2)$$

where the subscripts "s" and "c" identify flux components associated with the soil and canopy, R_n (W m^{-2}) identifies the net radiation, G_0 (W m^{-2}) the soil heat flux, H and λE (W m^{-2}) are turbulent fluxes of sensible and latent heat, respectively.

Net radiation components in Eqs. (1) and (2) are modeled by analyzing separately the transport of short-wave radiation, R_s (Campbell and Norman, 1998) and long-wave radiation (Ross, 1975) within the canopy–soil system. Following this approach, radiation extinction processes are parameterized as function of leaf area index, LAI (m^2 m^{-2}), and vegetation class-specific parameters (i.e., leaf size, vegetation height and clumping characteristics) as described in detail in the Appendix of Li et al. (2005). G_0 is computed as a fraction of $R_{n,s}$ following the semi-empirical diurnal relationship proposed by Santanello and Friedl (2003). The TSEB model takes a physically based approach using LST to constrain the H flux estimates, which are modeled following a temperature gradient-transport in-series resistance network between the soil, canopy, and atmosphere.

In this framework, the separation between soil and canopy heat fluxes is achieved by partitioning the remotely observed surface radiometric temperature, T_{RAD} (K), into canopy, T_c (K), and soil, T_s (K), contributions using the equation:

$$T_{RAD}(\theta) = \{f_c(\theta)T_c^4 + [1 - f_c(\theta)]T_s^4\}^{1/4} \quad (3)$$

where $f_c(\theta)$ is the vegetation coverage apparent at the view zenith angle (θ) of the thermal radiometer, derived from remote sensing estimates of LAI (m^2 m^{-2}).

Latent heat from the canopy is estimated under the first-guess hypothesis of unstressed conditions using the Priestley and Taylor (1972) formulation. If this results in negative soil evaporation, derived as a residual of Eq. (1), this hypothesis is relaxed iteratively until $\lambda E_s > 0$ is obtained, as condensation under daytime clear-sky conditions is unlikely. System (soil + canopy) latent heat estimates at the sensor overpass time are upscaled to daytime evapotranspiration (ET) assuming a self-preservation of the evaporative fraction, $\Lambda = \lambda E/(R_n - G_0)$, during daytime hours (Brutsaert and Sugita, 1992). Daytime values of net radiation and soil heat flux are derived from hourly estimates. A correction multiplicative coefficient of 1.1 for Λ is introduced to account for a 10% systematic underestimation of daytime average Λ from values estimated around midday (Brutsaert and Sugita, 1992).

Direct use of absolute T_{RAD} measurements in TSEB to determine the surface–air temperature gradient can lead to significant biases in flux estimates, mainly due to uncertainty in absolute calibration of TIR measurements from remote sensors (Jacob et al., 2004). Even using perfectly calibrated and corrected T_{RAD} maps, TSEB may produce poor flux estimates if the air temperature observations are acquired over non-representative surfaces. This issue was addressed by Anderson et al. (1997), who implemented the TSEB in time-differential mode within the ALEXI regional modeling framework. In ALEXI, the TSEB is applied at two times during the morning hours (generally after sunrise and close to local noon). The resulting time-integrated morning sensible heat flux is coupled with a simple slab model of atmospheric boundary layer growth (McNaughton and Spriggs, 1986) to internally simulate land–atmosphere feedback on near-surface air temperature. In this mode, ALEXI flux estimates are relatively insensitive to both time-invariant biases in LST data and biases in non-representative air temperature fields (Anderson et al., 2007). However, this method can be only applied to satellite systems that sample the morning surface temperature rise, such as geostationary platforms, which are typically of relatively coarse spatial resolution.

For higher spatial resolution mapping, Norman et al. (2003) introduced the ALEXI flux disaggregation procedure, DisALEXI. DisALEXI uses the fluxes assessed at continental scale by the ALEXI model to constrain sub-pixel fluxes obtained by applying the TSEB to higher resolution TIR data, typically from polar orbiting systems – in this case from Landsat and MODIS. An initial guess air temperature map is iteratively altered until the aggregated daytime fluxes retrieved by DisALEXI match the ALEXI fluxes at the scale of the ALEXI grid (Cammalleri et al., 2013).

2.2. Fusion of ET maps at different spatial resolution

The Spatial and Temporal Adaptive Reflectance Fusion Model (STARFM), developed by Gao et al. (2006), can be used to combine temporally sparse Landsat and daily MODIS ET maps in order to retrieve Landsat-like images at daily timesteps. This fusion methodology allows us to combine ET maps generated with satellite data at different overpass times. Consistency at coarse resolution (10-km) between ET maps is ensured by using the ALEXI (GOES) retrievals as common normalization field for both Landsat and MODIS DisALEXI applications as described in the previous section.

Estimation of ET at Landsat resolution (ET_L) for a generic day (d) between Landsat overpasses is based on a weighting function applied within a specified search window:

$$ET_L\left(\frac{x_w}{2}, \frac{y_w}{2}, d\right) = \sum_{i=1}^{w}\sum_{j=1}^{w} W_{ij}[ET_M(x_i, y_j, d) + ET_L(x_i, y_j, d_0) - ET_M(x_i, y_j, d_0)] \quad (4)$$

where ET_M is a MODIS ET retrieval (available daily), w is the search window size, x_i and y_j give the pixel location in coregistered Landsat and MODIS scenes, d_0 is the acquisition date for the Landsat/MODIS pair used to train the fusion, and the weighting factor, W, is parameterized in terms of the spatial, temporal and magnitude similarities with neighbor pixels (assuming that similar surface types under similar environmental/moisture conditions exist within the search window at both MODIS and Landsat scales) as described in Gao et al. (2006).

As expressed by Eq. (4), a single pair of Landsat/MODIS ET images (obtained on day d_0) is used in the fusion procedure. This choice is more effective than using two bounding pairs of training images because it better captures ET changes due to variations in meteorological forcing (e.g., a rainfall event) that occurred between two successive Landsat acquisitions. The optimal training pair is selected by an automated process that searches the complete set of Landsat/MODIS ET map pairs available at Landsat imaging times and identifies the day d_0 where the MODIS ET estimates are most highly correlated with the MODIS ET field on day d. A schematic description of this procedure is reported in Fig. 1, and further details are provided in Cammalleri et al. (2013).

The quality of the predicted Landsat-like ET maps strongly depends on the spatial heterogeneity of the geographic region and on the spatial scale of the moisture perturbations. STARFM relies on temporal information from pure, homogeneous patches of land cover at the MODIS pixel scale. These homogeneous MODIS pixels should be able to cover the whole range of conditions available at Landsat spatial resolution (i.e., including wet fields with full vegetation coverage) in order to obtain accurate Landsat-like predictions. Obviously, predictions may be degraded when STARFM is applied to heterogeneous fine-grained landscapes, including small-scale agricultural fields that are not well represented at the MODIS spatial

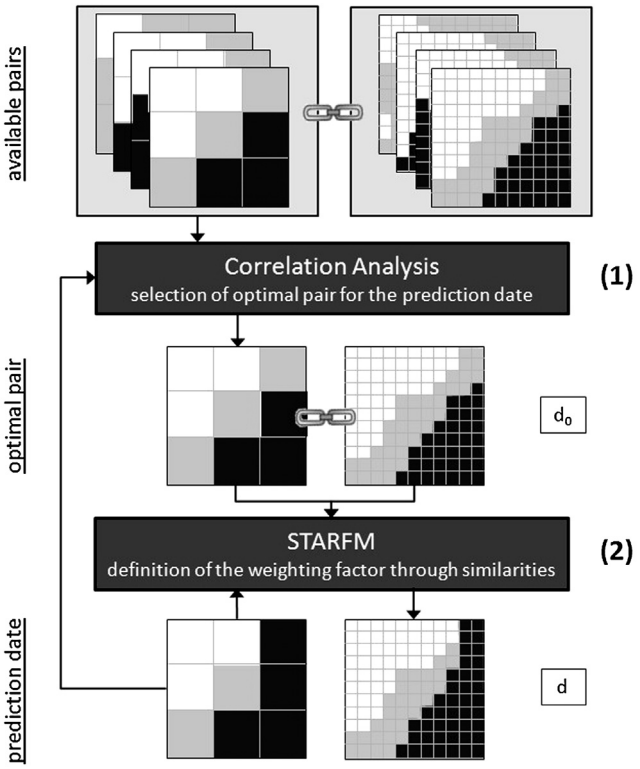

Fig. 1. Schematic description of the STARFM data fusion procedure. In step (1), a correlation analysis is performed between the MODIS ET map on the prediction date and all the available MODIS maps at the Landsat overpass dates to identify the optimal Landsat/MODIS pair. In the step (2), a weighting function is determined using the optimal pair acquired on day d_0 and a Landsat-like ET map is predicted for day d.

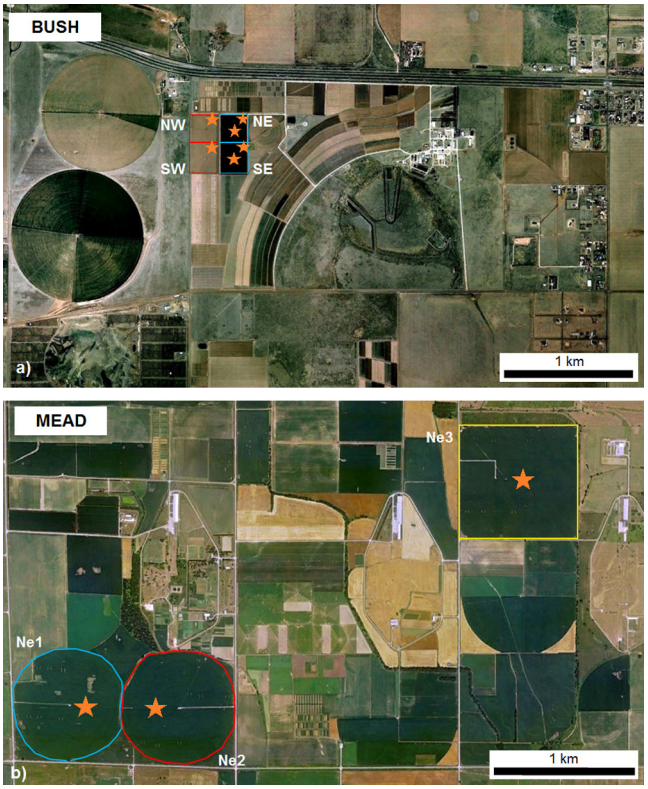

Fig. 2. Location of the study fields within the two study areas. Panel (a) shows the BUSH site (Google Earth, April 2006) and panel (b) shows the MEAD study area (Google Earth, April 2004). Stars demarcate the location of the eddy covariance flux towers.

scale (Hilker et al., 2009). Similarly, fine-scale alternation of wet and dry areas, such as in the case of sparsely irrigated fields within a dry environment, may be not fairly captured in the fused ET map if these features do not have substantial representation at the MODIS pixel scales.

3. Materials

3.1. Experimental sites

Two study sites were selected to evaluate the performance of the Landsat–MODIS data fusion methodology over a mixture of rainfed and irrigated agricultural areas: (1) the Bushland, TX study area (BUSH), located west of Amarillo, TX (35°11′ N, 102°4′ W) and containing both irrigated and rainfed cotton fields; (2) the Mead, NE study area (MEAD), located east of Wahoo, NE (41°11′ N, 96°27′ W) and mainly occupied by corn and soybean fields (Fig. 2). The BUSH study area was the focus of the 2008 Bushland Evapotranspiration and Agricultural Remote Sensing Experiment (BEAREX08), conducted at the USDA-ARS Conservation and Production Research Laboratory (CPRL) during June–August 2008 (Evett et al., 2012). During the experiment, flux measurements were carried out over a pair of adjacent irrigated/unirrigated cotton fields. Both fields measured approximately $220 \times 220\,m^2$ and had an area of about 4.7 ha (see Fig. 2a). Each field was subdivided into two areas: NE and SE (irrigated), and NW and SW (unirrigated). The MEAD study area is continuously monitored by three AmeriFlux installations located at the University of Nebraska Agricultural Research and Development Center (Verma et al., 2005). Data from 2003 were used in this study, when all three sites were planted in corn. Fields Ne1 (48.7 ha) and Ne2 (52.4 ha) were both irrigated (center-pivot), whereas field Ne3 (65.4 ha) was rainfed (see Fig. 2b). All sites at MEAD are within 1.6 km of each other and are located on silty clay loam soils (Kucharika and Twine, 2007). In 2003, the corn was planted around May 15 in all three fields. Additional details on planting density and crop management at MEAD can be found in Verma et al. (2005).

These two study areas have different climates, with the MEAD site characterized by a humid continental climate, and BUSH a semi-arid climate often under strong advection. In general, BUSH has a higher annual average temperature than MEAD (14 and 10.5 °C, respectively), and a lower annual precipitation rate (500 vs. 700 mm, respectively). During the May–September period, the average temperatures of the two sites differ slightly (≈1 °C), while the difference in precipitation is more significant (≈30 mm) (http://www.drought.unl.edu). Another interesting distinction is that irrigated fields at BUSH site are affected by strong local horizontal advection of dry and warm air from adjacent unirrigated areas under windy conditions, which can cause very large evaporative fluxes (Alfieri et al., 2012; Prueger et al., 2012). Additionally, due to the small size, the BUSH field sites are contained within the same MODIS TIR pixel and occupy just a fraction of the MODIS pixel area, while the size of the MEAD fields is comparable to the MODIS spatial resolution (see Fig. 2).

Meteorological data over the two study areas were obtained from the Fifth-Generation Pennsylvania State University/National Center for Atmospheric Research Mesoscale Model (Dudhia, 1993) at a spatial resolution of 36-km, while insolation data were obtained from hourly GOES-based products at 20-km resolution (Otkin et al., 2005). Daily ET maps at 10-km spatial resolution, used as the normalization basis for DisALEXI, were obtained from routine estimates provided by the ALEXI model on the CONUS grid (Anderson et al., 2007).

Model inputs describing vegetation characteristics at the two sites (i.e., canopy height range, leaf size and clumping factor) were derived from generalized land-cover maps. In particular, the 1-km land-cover classification developed by University of Maryland (UMD) was used for ALEXI and DisALEXI/MODIS estimates, whereas the 30-m National Land Cover Data (NLCD) map (Homer et al., 2007) was used in DisALEXI/Landsat. Both land-cover maps yielded a generic classification of "cropland" over the study sites – no information about specific crop type was provided to the modeling system.

3.2. Measurement of surface energy fluxes

At both the BUSH and MEAD experiment sites, flux towers were installed to monitor surface energy fluxes. At BUSH, eddy covariance flux data were collected at two locations per field within the NE and SE fields, and one location per field in the NW and SW fields (see Fig. 2a). The irrigated fields were also equipped with lysimeters; however, these data were not used in the current analysis to maintain consistency between the BUSH and MEAD experiments. Each micrometeorological system was equipped with a sonic anemometer (CSAT-3, Campbell Scientific Inc., Logan, UT) to measure the orthogonal wind velocity components and an open-path infrared gas analyzer (LI-7500, Li-Cor Inc., Lincoln, NE) to measure both water vapor and carbon dioxide concentration at a height of about 2.5 m above the ground. Additional instruments at each site include a four-component net radiometer (CNR-1, Kipp and Zonen, Delft, The Netherlands), three soil heat flux plates (HFT-3, Radiation Energy Balance Systems, Bellevue, WA) buried at a depth of 8 cm paired with soil thermocouples (Omega Engineering Inc., Stamford, CT) and soil moisture probes (HydraProbe, Stevens Water Monitoring Systems, Portland, OR) for correction of heat storage above the plates. The flux data were post-processed using the full complement of standard corrections and adjustments, including two-dimensional rotation, frequency response attenuation, and correcting the effects of heat and water vapor density (Webb–Pearman, Leuning procedure, Webb et al., 1980). Further details on experimental setup are provided in Alfieri et al. (2012).

Surface flux measurements at MEAD were collected using similar sensor systems deployed at each of the three sites: a 3D sonic anemometer (R2, Gill Instruments Ltd., Lymington, UK) and a closed-path infrared CO_2/H_2O gas analyzing system (LI6262, Li-Cor Inc., Lincoln, NE). These instruments were installed at a height of 3.0 m above the ground when the canopy was shorter than 1 m, and later moved to a height of 6.0 m until harvest. Net radiation at 5.5 m (Q-7.1, Radiation and Energy Balance Systems Inc., Seattle, WA), and soil heat flux (at 0.06 m depth; HFT-3, Radiation & Energy Balance Systems Inc., Seattle, WA) were also measured and corrected for above-plate heat storage. Details on measurements and calculations are given in Suyker and Verma (1993).

3.3. MODIS data processing

MODIS standard products were used to obtain DisALEXI inputs at 1-km resolution for daily estimates. More specifically, LAI maps were generated from the 8-day composite (MOD15A2, Collection 5) product (Myneni et al., 2002) and interpolated using a spline function to daily timesteps. The Terra (MOD11_L2) instantaneous swath LST product (Wan and Li, 1997) was used to derive T_{RAD} maps. Effects of off-nadir pixel smearing were reduced by applying a thermal image sharpening procedure (TsHARP; Kustas et al., 2003) using the MODIS 1-km composite NDVI product. The MOD35 cloud mask product (Ackerman et al., 1998) was used to detect clear-sky pixels, assuming a threshold at 99% confidence interval. As result of this data screening, about 55% and 48% of the images were considered cloudy on the experimental fields for BUSH and MEAD, respectively, with an average actual average revisit interval of 3.0 and 2.1 days.

3.4. Landsat data processing

Landsat data were collected over the two study areas (BUSH: path 30, row 36; MEAD: path 28, row 31): five predominantly clear scenes were acquired over BUSH during the period June–August 2008 (DOY 155, 187, 203, 219, 235) with an average frequency of 20 days and a maximum gap of 32 days; and six scenes were acquired over MEAD between May and September 2003 (DOY 127, 151, 191, 207, 239, 255) with an average frequency of 26 days and a maximum gap of 40 days. All the scenes were collected by the Landsat 5 satellite except for one scene on DOY 151 over MEAD, which was acquired by Landsat 7 just before the scan line corrector failure.

Raw Landsat shortwave data were calibrated and atmospherically corrected to surface reflectance using the Landsat Ecosystem Disturbance Adaptive Processing System (Masek et al., 2006); LAI maps at 30-m resolution were obtained from surface reflectance using a regression tree approach trained by MODIS 1-km LAI sample data, as described in Gao et al. (2012). Landsat LST maps, at the native spatial resolution of 120-m (Landsat 5) or 60-m (Landsat 7), were derived from thermal band observations by atmospherically correcting at-sensor brightness temperature via MODTRAN (Berk et al., 1989). Finally, these LST maps were sharpened to the 30-m resolution of the Landsat optical bands using the TsHARP sharpening procedure (Kustas et al., 2003).

4. Results and discussion

The high spatial resolution of Landsat data permits a direct evaluation of the DisALEXI outputs in comparison with flux tower observations. In Fig. 3, comparisons between daily observed and modeled fluxes on the Landsat overpass dates for the BUSH (Fig. 3a) and MEAD (Fig. 3b) experiments are shown. Note that some flux towers did not generate usable data for all the Landsat dates. Given that the final goal of the analysis is to accurately reproduce daily ET fluxes, the capability to correctly partition the surface energy fluxes at the imaging dates is crucial for the consequent reconstruction of the ET timeseries. The plots in Fig. 3 demonstrate good correspondence between daily observations and model outputs for all the main energy budget terms at both the BUSH and MEAD sites, and a similar performance of the model over the two sites.

These results are further corroborated by the statistical performance metrics derived for each flux and summarized in Table 1, showing similar model accuracy in the two experiments. At MEAD the mean absolute error, MAE, for λE is 1.3 MJ m^{-2} d^{-1} (0.53 mm d^{-1} in terms of daily ET), while MAE is 1.4 MJ m^{-2} d^{-1} (0.57 mm d^{-1}) at BUSH. The slight underestimation of λE obtained at both BUSH and MEAD (mean bias error, MBE, equal to −0.8 and −0.6 MJ m^{-2} d^{-1}, respectively) may reflect limitations of the Priestley–Taylor equation used for modeling canopy transpiration in capturing advective contributions to the fluxes. Another possible reason of the negative bias can be the systematic error in daytime upscaling procedure (Van Niel et al., 2012). The average errors obtained in the two sites are at the lower end of the typical error range associated with published remote sensing methods, as reported in Kalma et al. (2008). Additionally, in view of the magnitude of the fluxes recorded in the two experiments, especially in the central part of the growing season in irrigated fields, the relative accuracy of direct retrievals with DisALEXI on Landsat dates can be considered comparable to the typical uncertainty of eddy covariance technique (Wilson and Baldocchi, 2000).

In the next step, a continuous stream of daily Landsat-like ET maps was produced for each experiment using STARFM and compared with flux tower observations. The irrigated and rainfed

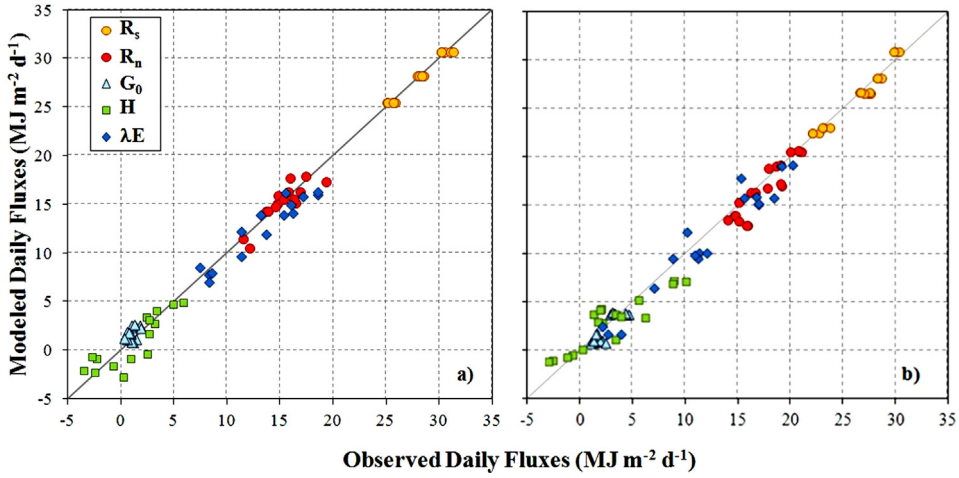

Fig. 3. Scatterplot of observed vs. modeled daytime integrated surface fluxes on Landsat overpass dates. Panel (a) shows the results for BUSH experiment, while panel (b) reports the results for MEAD sites.

fields in each experiment were analyzed separately to highlight effects of irrigation supplies on model accuracy under different meteorological conditions. The plot in Fig. 4 shows comparisons between observed and modeled ET datastreams for: BUSH rainfed (NW + SW, Fig. 4a) and irrigated (NE + SE, Fig. 4b) fields, MEAD rainfed site (Ne3, Fig. 4c) and MEAD irrigated fields (Ne1 + Ne2, Fig. 4d). In those plots, the observed fluxes represent the average tower observations in the rainfed or irrigated fields, while the modeled values represent a spatial average over all 30-m pixels within a given field or set of fields. The ET fluxes were converted to units of mass flux (mm d^{-1}), as is customary for agricultural water use estimates.

Figure 4 highlights the similarity in model performance between irrigated and rainfed fields for each experiment in the first part of season, when the plant coverage is still low and rainfall events are the main water supply, with larger discrepancies later in the season (after DOY 195 in BUSH and DOY 215 in MEAD) when water stress occurs in the rainfed fields. These late-season differences are more evident at the BUSH site than at MEAD, which may be explained by the difference in climate between the two regions. In fact, the dry climate of BUSH likely causes strong water stress in the absence of irrigation, severely limiting plant growth (thus transpiration fluxes), whereas the temperate climate over MEAD appears to have less impact on plant growth. Another notable difference is observed between irrigated fields at BUSH and MEAD during the irrigation stage. Irrigation events in the BUSH NE + SE fields (highlighted by the arrows in Fig. 4b) result in spikes in the observed ET data on the dates of irrigation (e.g., DOY 193, 199, 204). This fast response to irrigation is not visible in the MEAD Ne1 + Ne2 plot (Fig. 4d). The extremely high values observed in BUSH (e.g., 8–10 mm d^{-1} during DOY 193, 199 and 204) can be partially explained by a period of strong advection that occurred during the experiment, causing very high soil evaporation values following irrigation events. While eddy covariance observations are not completely reliable during irrigation days, these soil evaporation spikes were also confirmed by microlysimeter observations (Agam et al., 2012).

A quantitative analysis of the fused daily ET datastream is summarized in Table 2. The MAE in ET is 0.9–1.0 mm d^{-1} for the MEAD sites and BUSH NW + SW (unirrigated) field, while a higher MAE (1.51 mm d^{-1}) is obtained for the BUSH irrigated field. The root mean square error, RMSE, suggests similar performance at each site, with slightly higher errors for BUSH compared to the MEAD sites. Overall, the lower absolute accuracy (higher MAE and RMSE) obtained for BUSH NE + SE (irrigated) compared to the other sites is explained in part by the periodic high ET values observed directly after irrigation, which were systematically underestimated by the model. Additionally, the higher magnitude of ET in this field compared to the other sites leads to higher errors. Indeed the relative error (RE, MAE normalized to observed average) for BUSH NE + SE is similar to the values for BUSH NW + SW and MEAD Ne3 (see Table 2). These values are in the range of accuracy of typical eddy covariance installations (15–30%) as reported in

Table 1
Summary of the statistical indices quantifying DisALEXI model performance on Landsat imaging dates (5 days for BUSH and 6 days for MEAD) for daytime integrated surface fluxes.

Flux	N	$\bar{O}$ (MJ m^{-2} d^{-1})	MAE (MJ m^{-2} d^{-1})	RMSE (MJ m^{-2} d^{-1})	MBE (MJ m^{-2} d^{-1})
BUSH					
R_s	15	27.9	0.3	0.3	0.0
R_n	15	15.2	0.8	1.0	−0.1
G_0	15	1.0	0.8	0.9	0.7
H	15	1.1	1.2	1.5	−0.2
λE	15	13.2	1.4	1.4	−0.8
MEAD					
R_s	18	26.3	0.5	0.6	0.1
R_n	18	17.3	1.0	1.3	−0.6
G_0	18	2.2	0.6	0.7	−0.2
H	18	2.9	1.5	1.7	0.2
λE	18	12.2	1.3	1.5	−0.6

N, number of observations; $\bar{O}$, mean observed flux; MAE, mean-absolute error between the modeled and observed quantities; RMSE, root mean square error; MBE, mean bias error.

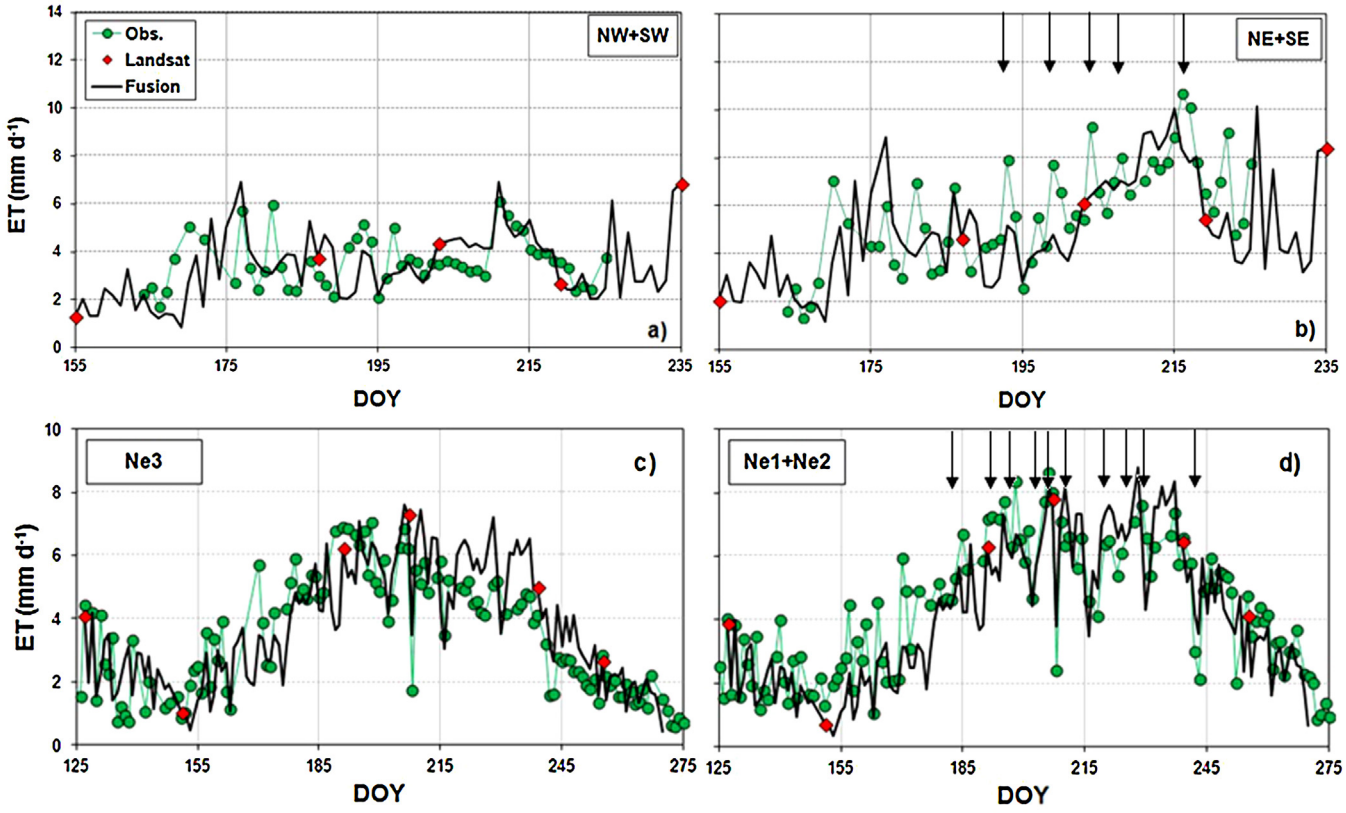

Fig. 4. Comparison of STARFM modeled (black line, Fusion) and flux tower observed (green dots, Obs.) time-series of daily ET for: BUSH rainfed (a) and irrigated (b) fields, and MEAD rainfed (c) and irrigated (d) sites. Red diamonds (Landsat) represent DisALEXI estimates at Landsat overpass dates. Arrows in (b) and (d) highlight the irrigation dates. (For interpretation of the references to color in this figure legend, the reader is referred to the web version of this article.)

Allen et al. (2011). The underestimation of observed ET values in irrigated fields is also reflected in the negative MBE obtained in both NE + SE and Ne1 + Ne2 (−0.46 and −0.42 mm d^{-1}, respectively). For the MEAD Ne1 + Ne2 irrigated fields, the underestimation is primarily observed during the rainy period around DOY 170 (see Fig. 4d) and was mainly driven by the absence of MODIS data across the rainfall event due to persistent cloud coverage.

In comparison with expected observational errors, the fusion model seems to reproduce the general ET trends at all the study sites reasonably well, including the relatively higher fluxes observed in irrigated fields in comparison to rainfed fields late in the season. The ET dynamics in the rainfed fields are reproduced on a day-to-day basis with an error of about 1 mm^{-1} and a small bias, which is comparable to the accuracy typically required for agricultural management at field scale (see e.g., Seguin et al., 1999). This result is mainly due to the fact that in these fields the main hydrological input is the rainfall. Given that rainfall generally occurs at a spatial scale greater than the MODIS TIR pixel resolution, the low-resolution data stream is able to capture the dynamics in water availability and STARFM is able to transfer this information to the field scale maps. The only notable exceptions are those periods when MODIS data were not available due to persistent clouds. In these cases (e.g., around DOY 170 in MEAD Ne1 + Ne2 and DOY 180 in BUSH NW + SW), the model tends to underestimate the actual ET by underestimating the soil evaporation following rainfall events. The underestimation during irrigation events results instead in slightly higher average errors over the BUSH irrigated field, with a MAE of 1.51 mm d^{-1} and a negative bias (MBE = −0.46 mm d^{-1}). The inability of the fusion results to reproduce the spikes in ET observed in the BUSH irrigated field can be ascribed to the very small size of the irrigated field, and the fact that this field was not representative of conditions in the surrounding areas, which was largely rainfed agriculture, urban or natural vegetation. In cases where no similar homogeneous areas are present at the 1-km scale, the information content conveyed by the MODIS data stream is likely limited to large rainfall events. Isolated, sub-pixel irrigation events – as in BUSH NE + NW – cannot be expected to be well reproduced by data fusion if the irrigation events cannot be captured at the MODIS pixel scale. Additionally, the strong advective conditions that occurred on a few of the days during BEAREX08 lead to high rates of ET from the irrigated fields directly after irrigation, which cannot be easily resolved at the MODIS spatial scale or with the Landsat temporal frequency. This issue fortunately occurs only on few days during the experiment, due the rapid decay in direct soil

Table 2
Statistical indices of data fusion model performance for the daily ET datastream. Relative error, RE, was obtained by dividing MAE with observed average flux. Other indices are described in Table 1.

Index	BUSH		MEAD	
	NE + SE (irrigated)	NW + SW (rainfed)	Ne1 + Ne2 (irrigated)	Ne3 (rainfed)
MAE (mm d^{-1})	1.51	1.01	0.91	0.90
RMSE (mm d^{-1})	1.81	1.29	1.11	1.10
MBE (mm d^{-1})	−0.46	−0.04	−0.42	0.21
RE (%)	26.6	27.0	20.8	25.4

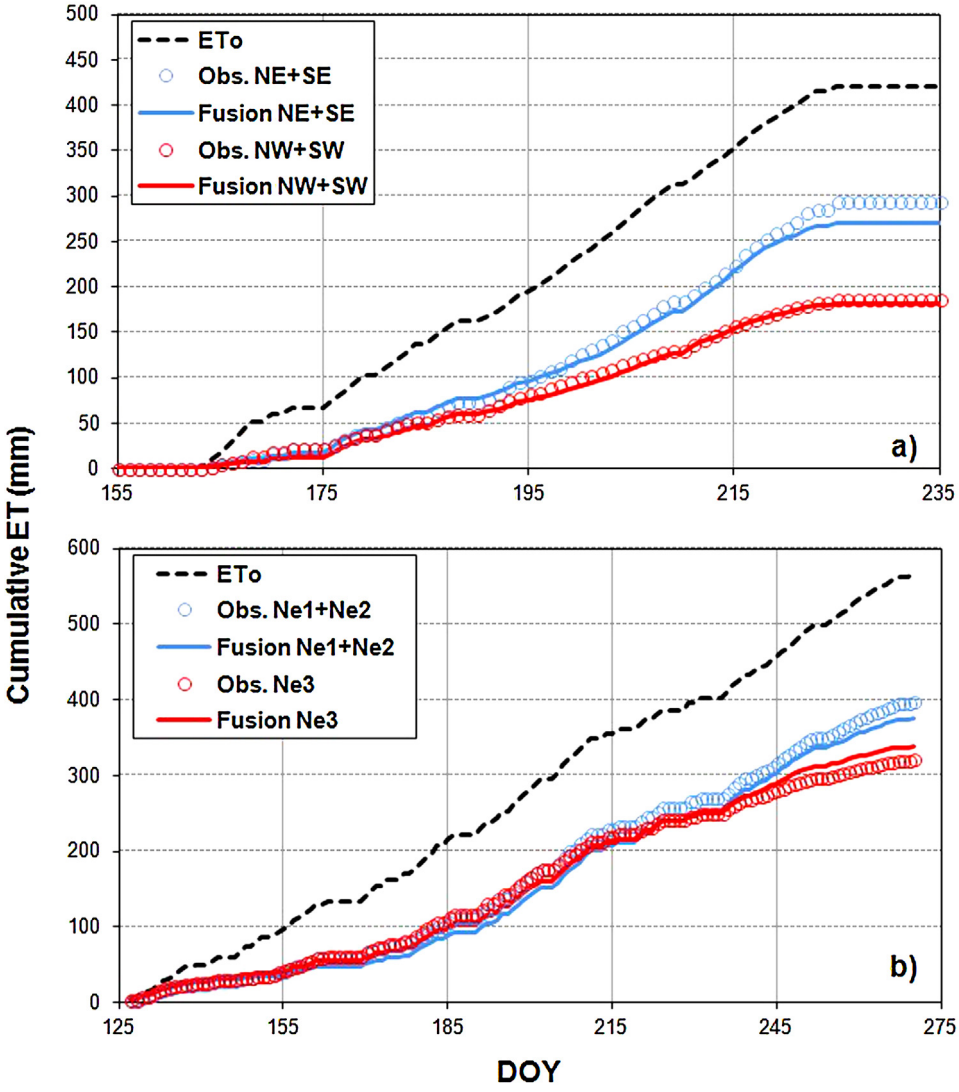

Fig. 5. Season-cumulative modeled (Fusion, continuous lines), measured (Obs., dots) and reference (ET_o, dotted line) ET for: (a) BUSH and (b) MEAD experimental sites.

evaporation following an irrigation event. It worth noting that the uncertainty of the eddy covariance observations over the irrigated field is also higher than those over the rainfed field due to advection effects (Alfieri et al., 2012). On the other hand, the model is able to reproduce the daily ET for the MEAD irrigated field with an accuracy similar to that for the rainfed field (MAE and RMSE equal to 0.9 and 1.1 mm d^{-1}, respectively). This is explained by the large size of the irrigated fields (50 ha each) at MEAD, and by the absence of spikes in observed ET under non-advective conditions.

The effects of this difference in model behavior between irrigated and rainfed fields can be also assessed at seasonal timescales by constructing cumulative ET plots as reported in Fig. 5. The observed season-cumulative ET in the rainfed and irrigated fields at the BUSH site (Fig. 5a) begin to diverge around DOY 190, while the corresponding plot for MEAD (Fig. 5b) shows notable differences between the two water management practices only at the very end of the season (after DOY 230). This behavior reflects the different effects of water stress under the two environments. In a semi-arid climate with strongly advective conditions (BUSH), the absence of irrigation greatly affects the cotton growth and water use, while at MEAD, due to the less severe meteorological conditions, the effect of water stress due to non-irrigation is manifested only in the late season with plant senescence. This can be also seen in terms of difference in the ratio between ET and reference ET (ET_o) for irrigated and rainfed fields, which is larger for BUSH (0.65–0.45) than for MEAD (0.68–0.55).

Overall, the data fusion approach reproduces the observed differences between cumulative ET in rainfed and irrigated fields in both experiments; the retrieved accuracy of modeled cumulative ET (complement to 1 of the relative error, ranging between 0.92 and 0.95) fulfill the general requirements in modeling seasonal water use since the errors are non-systematic and not accumulative (Kalma et al., 2008). Additionally, overall accuracy is in line with the best performance of validation experiments reported in Bastiaanssen et al. (2005) over agricultural landscapes. The capability of the model to reproduce cumulative ET even for the BUSH irrigated field is justified by the small number of days affected by the underestimation of ET during irrigation events. From this point of view, no significant difference was observed in the performance of the methodology between irrigated and rainfed fields, as well as for the two study sites.

In both Figs. 4 and 5, the main differences between irrigated and rainfed fields occur in July for BUSH and in September for MEAD. Focusing on these periods, monthly average ET maps for the two

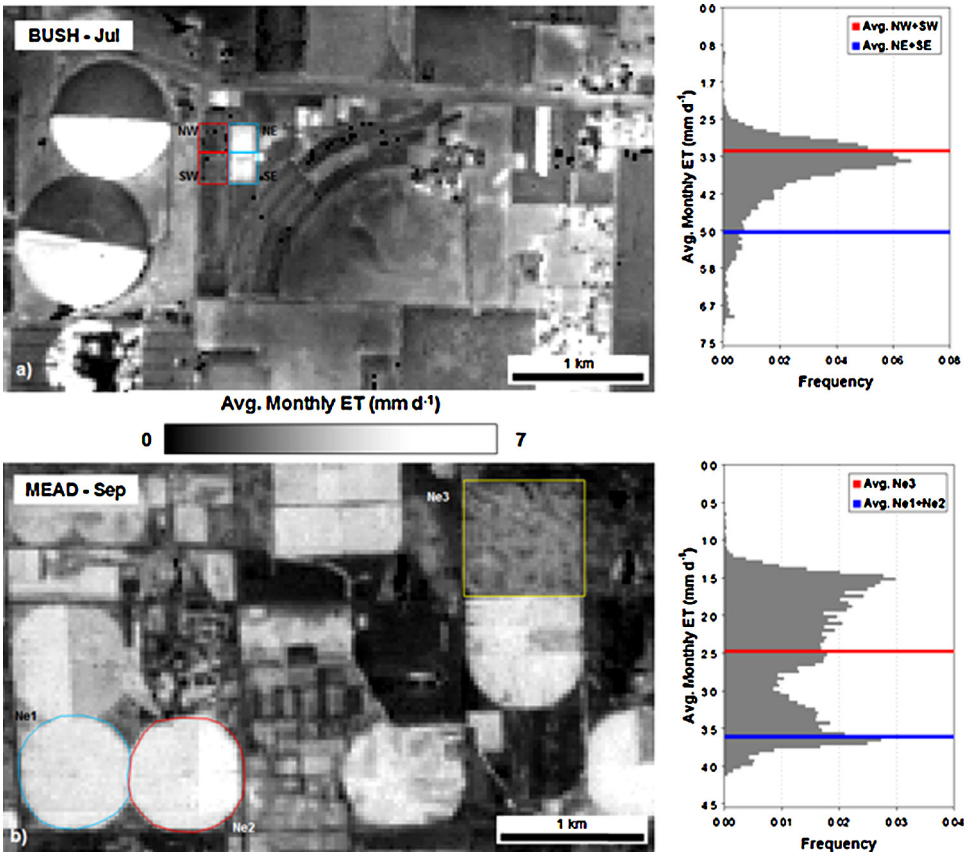

Fig. 6. Maps of monthly average ET during the irrigation period. Panel (a) depicts average ET in BUSH during July, while panel (b) reports September average ET in MEAD. Histograms on the side of each image show the frequency distribution of ET values within the two sub-areas, as well as the average value on the irrigated/rainfed fields.

sub-periods are illustrated in Fig. 6. Additionally, a frequency histogram for each map is included on the side of the image, as well as the average value observed in the two experimental fields. The monthly average ET map for the BUSH site (Fig. 6a) during July further confirms the arid condition of the areas surrounding the irrigated field, with the notable difference of two additional irrigated areas at the extreme west edge of the scene. The histogram shows how the soil moisture conditions in the rainfed field (NW + SW) are consistent with the peak in the distribution of ET values, while the high ET associated with the irrigated field (NE + SE) is representative of a much smaller percentage of pixels within the scene. On the other hand, the monthly average ET map in September over MEAD (Fig. 6b) is almost equally comprised of high and low ET values, with a clear bimodal frequency distribution. The peak corresponding to irrigated areas is narrow, confirming the leveling effect of irrigation supply on ET, while the broader peak associated with non-irrigated areas can be sub-divided into more dry areas (e.g., bare soil fields) and water stressed crop fields.

5. Summary and conclusions

Time-continuous and robust estimation of daily evapotranspiration, ET, at field scales using thermal remote sensing-based approaches can be of substantial benefit for agricultural water management worldwide, facilitating optimal use of limited freshwater resources. Due to the current lack of high spatiotemporal resolution thermal data, the STARFM data fusion approach has been identified as a valuable means for combining ET maps obtained using DisALEXI applied to high spatial resolution Landsat data and to high temporal frequency MODIS images. The major challenge for data fusion methodologies is in heterogeneous areas where rainfed and irrigated fields coexist, and irrigated areas represent a small fraction of the total area comprised in a MODIS TIR pixel.

The results reported here indicate that the accuracy of the DisALEXI model applied using actual Landsat data is consistent between irrigated and rainfed crop fields in areas with contrasting climatic conditions including a region in the semi-arid strongly advective region in the Texas Panhandle (BUSH) and a temperate experimental site in Eastern Nebraska (MEAD). This suggests that high resolution land surface temperature maps are able to correctly constrain the surface energy budget, capturing differences in evapotranspirative fluxes between water stressed/unstressed crops at field scale. The DisALEXI model accuracy for daytime-integrated ET on Landsat overpass dates was 1.3 MJ m^{-2} d^{-1} (≈0.5 mm d^{-1}), with a slightly negative bias of −0.7 MJ m^{-2} d^{-1} (0.3 mm d^{-1}). Additionally, the time series of Landsat-like ET images obtained by fusing periodic Landsat estimates with daily MODIS data showed an agreement with ET from in situ flux tower measurements on the order of 1 mm d^{-1}, which is generally suitable for the use in agricultural studies. General trends in the ET observed timeseries were captured by the model in both irrigated and rainfed fields, as well as the day-to-day dynamics. The analysis of growing season cumulative ET data further confirms the ability of the data fusion approach to discriminate between the responses of irrigated and rainfed fields in terms of ET fluxes, also of benefit for agricultural applications. The differences between ET in irrigated and rainfed fields, which were more marked at the BUSH site and less evident at the MEAD location, were fairly well captured by the model, since the error in cumulative ET (∼5%) is smaller than the difference observed between the two water management conditions. This suggests that the effects of irrigation on plant water use were correctly identified and the two water stress conditions were correctly discriminated.

From this analysis, some general conclusions are reached regarding the reliability of continuous ET estimates over heterogeneous agricultural areas. The fusion of MODIS and Landsat data is effective when the main forcing is rainfall, which is in general resolved at the MODIS spatial resolution. However, short timescale variability in ET during periods of persistent cloud cover cannot be captured using TIR techniques. In persistently cloudy regions of the globe, ET estimation may benefit from additional fusion of ancillary daily soil moisture information provided at coarser spatial resolution using microwave techniques (Holmes et al., 2013).

Spatial patterns in soil moisture variability over the landscape may also impact the success of fused Landsat/MODIS ET retrievals, particularly when the target field size is significantly smaller than the MODIS pixel resolution and field conditions differ substantially from those of the surrounding area. In this specific case study, this issue primarily arose at the BUSH site during days directly following an irrigation event, because the localized decrease of surface temperature due to increased soil evaporation and canopy transpiration within the small irrigated fields did not substantially modify the aggregate land-surface temperature at the MODIS thermal pixel scale. This generally caused an underestimation of daily ET due to the underestimation of soil evaporation by the model. Fortunately, this limitation was confined to a few days following irrigation events, and it seems to be exacerbated in a dry climate under strong advection as observed at the BEAREX08 site in Bushland, TX. The absence of such features for the MEAD site supports this conclusion, where neither observed nor modeled data show significant increase in ET after irrigation events.

The results at longer time scales (e.g., cumulative seasonal ET) confirm that the model is suitable for clearly distinguishing the two irrigation schemes over different meteorological conditions, which will be of benefit for water management applications. The absence of systematic errors at daily scale resulted in good agreement in seasonal total water loss (errors of 5–8%), suggesting that seasonal scale estimates were not significantly compromised by the underestimation following irrigation events (cf., Fig. 5), mainly because the number of irrigation events were limited and impacts were relatively short-lived. The results from this study cover extreme cases in terms of both field size and climatic conditions, suggesting that the modeling approach tested here has potential for producing reliable daily ET for many agricultural landscapes. However, further substantial improvements in model accuracy at daily scale over small irrigated fields may be difficult to achieve in the near term, given limitations in current TIR data availability at this fine field scale. Over highly fragmented areas, only a higher temporal frequency of high resolution thermal data acquisition seems to be a suitable solution.

Acknowledgments

This work was supported in part by funding from NASA grant NNH11AQ82I. The authors would like to thank Dr. Shashi Verma for collection of the MEAD flux dataset, and collaborators at USDA-ARS CPRL for their support of the BEAREX'08 field experiment.

References

Ackerman, S.A., Strabala, K.I., Menzel, W.P., Frey, R.A., Moeller, C.C., Gumley, L.E., 1998. Discriminating clear sky from clouds with MODIS. J. Geophys. Res. 103 (D24), 32141–32157.

Agam, N., Evett, S.R., Tolk, J.A., Kustas, W.P., Colaizzi, P.D., Alfieri, J.G., McKee, L.G., Copeland, K.S., Howell, T.A., Chávez, J.L., 2012. Evaporative loss from irrigated interrows in a highly advective semi-arid agricultural area. Adv. Water Resour. 50, 20–30.

Alfieri, J.G., Kustas, W.P., Prueger, J.H., Hipps, L.E., Evett, S.R., Basara, J.B., Neale, C.M.U., French, A.N., Colaizzi, P., Agam, N., Cosh, M.H., Chávez, J.L., Howell, T.A., 2012. On the discrepancy between eddy covariance and lysimetry-based surface flux measurements under strongly advective conditions. Adv. Water Resour. 50, 62–78.

Allen, R.G., Pereira, L.S., Howell, T.A., Jensen, M.E., 2011. Evapotranspiration information reporting: I. factors governing measurement accuracy. Agric. Water Manage. 98 (6), 899–920.

Anderson, M.C., Norman, J.M., Diak, G.R., Kustas, W.P., Mecikalski, J.R., 1997. A two-source time-integrated model for estimating surface fluxes using thermal infrared remote sensing. Remote Sens. Environ. 60, 195–216.

Anderson, M.C., Norman, J.M., Mecikalski, J.R., Otkin, J.A., Kustas, W.P., 2007. A climatological study of evapotranspiration and moisture stress across the continental United States based on thermal remote sensing: 1. model formulation. J. Geophys. Res. 112, D10117.

Anderson, M.C., Kustas, W.P., Alfieri, J.G., Hain, C.R., Prueger, J.H., Evett, S.R., Colaizzi, P.D., Howell, T.A., Chávez, J.L., 2012a. Mapping daily evapotranspiration at Landsat spatial scales during the BEAREX'08 field campaign. Adv. Water Resour. 50, 162–177.

Anderson, W.B., Zaitchik, B.F., Hain, C.R., Anderson, M.C., Yilmaz, M.T., Mecikalski, J.R., Schultz, L., 2012b. Towards an integrated soil moisture drought monitor for East Africa. Hydrol. Earth Syst. Sci. 16, 2893–2913.

Bastiaanssen, W.G.M., Noordman, E.J.M., Pelgrum, H., davids, G., Thoreson, B.P., Allen, R.G., 2005. SEBAL model with remotely sensed data to improve water resources management under field conditions. J. Irrig. Drain. Eng. 131 (1), 85–93.

Berk, A., Bernstein, L.S., Robertson, D.C., 1989. MODTRAN: A Moderate Resolution Model for LOWTRAN 7. GL-TR-89-0122. Air Force Geophysics Lab, Bedford, MA, pp. 38.

Brutsaert, W., Sugita, M., 1992. Application of self-preservation in the diurnal evolution of the surface energy budget to determine daily evaporation. J. Geophys. Res. 97 (D17), 18377–18382.

Cammalleri, C., Anderson, M.C., Ciraolo, G., D'Urso, G., Kustas, W.P., La Loggia, G., Minacapilli, M., 2012. Applications of a remote sensing-based two-source energy balance algorithm for mapping surface fluxes without in-situ air temperature observations. Remote Sens. Environ. 124, 502–515.

Cammalleri, C., Anderson, M.C., Gao, F., Hain, C.R., Kustas, W.P., 2013. A data fusion approach for mapping daily evapotranspiration at field scale. Water Resour. Res. (accepted for publication).

Campbell, G.S., Norman, J.M., 1998. An Introduction to Environmental Biophysics. Springer-Verlag, pp. 286.

Dudhia, J., 1993. A nonhydrostatic version of the Penn State/NCAR mesoscale model: validation tests and simulation of an Atlantic cyclone and cloud front. Mon. Weather Rev. 121, 1493–1513.

Evett, S.R., Kustas, W.P., Gowda, P.H., Anderson, M.C., Prueger, J.H., 2012. Overview of the Bushland Evapotranspiration and Agricultural Remote Sensing Experiment 2008 (BEAREX08): a field experiment evaluating methods for quantifying ET at multiple scales. Adv. Water Resour. 50, 4–19.

Gao, F., Masek, J., Schwaller, M., Hall, F., 2006. On the blending of the Landsat and MODIS surface reflectance: predicting daily Landsat surface reflectance. IEEE Trans. Geosci. Remote Sens. 44 (8), 2207–2218.

Gao, F., Anderson, M.C., Kustas, W.P., Wang, Y., 2012. Simple method for retrieving leaf area index from Landsat using MODIS leaf area index products as reference. J. Appl. Remote Sens. 6, 063554, http://dx.doi.org/10.1117/1.JRS.6.063554.

Hilker, T., Wulder, M.A., Coops, N.C., Sritz, N., White, J.C., Gao, F., Masek, J.G., Stenhouse, G., 2009. Generation of dense time series synthetic Landsat data through data blending with MODIS using a spatial and temporal adaptive reflectance fusion model. Remote Sens. Environ. 113, 1988–1999.

Holmes, T.R.H., Crow, W.T., Hain, C.R., 2013. Spatial patterns in timing of the diurnal temperature cycle. Hydrol. Earth Syst. Sci. 17, 3695–3706.

Homer, C., Dewitz, J., Fry, J., Coan, M., Hossain, N., Larson, C., Herold, N., McKerrow, A., VanDriel, J.N., Wickham, J., 2007. Completion of the 2001 National Land Cover Database for the Conterminous United States. Photogramm. Eng. Remote Sens. 73 (4), 337–341.

Jacob, F., Petitcolin, F., Schmugge, T.J., Vermote, E., Ogawa, K., French, A.N., 2004. Comparison of land surface emissivity and radiometric temperature derived from MODIS and ASTER sensors. Remote Sens. Environ. 90, 137–152.

Kalma, J.D., McVicar, T.R., McCabe, M.F., 2008. Estimating land surface evaporation: a review of methods using remotely sensed surface temperature data. Surv. Geophys. 29 (4–5), 421–469.

Kucharika, C.J., Twine, T.E., 2007. Residue, respiration, and residuals: evaluation of a dynamic agroecosystem model using eddy flux measurements and biometric data. Agric. For. Meteorol. 146 (3–4), 134–158.

Kustas, W.P., Norman, J.M., 1999. Evaluation of soil and vegetation heat flux predictions using a simple two-source model with radiometric temperatures for partial canopy cover. Agric. For. Meteorol. 99, 13–29.

Kustas, W.P., Norman, J.M., Anderson, M.C., French, A.N., 2003. Estimating subpixel surface temperatures and energy fluxes from the vegetation index–radiometric temperature relationship. Remote Sens. Environ. 85, 429–440.

Li, F., Kustas, W.P., Prueger, J.H., Neale, C.M.U., Jackson, T.J., 2005. Utility of remote sensing-based two-source energy balance model under low- and high-vegetation cover conditions. J. Hydrometeorol. 6, 878–891.

Liang, S., Wang, K., Zhang, X., Wild, M., 2010. Review on estimation of land surface radiation and energy budgets from ground measurement, remote sensing and model simulations. IEEE J. Sel. Topics Appl. Earth Observ. 3 (3), 225–240.

Masek, J.G., Vermote, E.F., Saleous, N.E., Wolfe, R.E., Hall, F.G., Huemmrich, K.F., Gao, F., Kutler, J., Lim, T.-K., 2006. A Landsat surface reflectance dataset for North America, 1990–2000. IEEE Geosci. Remote Sens. Lett. 3 (1), 68–72.

McNaughton, K.G., Spriggs, T.W., 1986. A mixed-layer model for regional evaporation. Boundary-Layer Meteorol. 34, 243–262.

Myneni, R.B., Hoffman, S., Knyazikhin, Y., Privette, J.L., Glassy, J., Tian, Y., Wang, J., Song, X., Zhang, Y., Smith, G.R., Lotsch, A., Friedl, M., Morisette, J.T., Votava, P.,

Nemani, R.R., Running, S.W., 2002. Global products of vegetation leaf area and fraction absorbed PAR from year one of MODIS data. Remote Sens. Environ. 83 (1–2), 214–231.
Norman, J.M., Kustas, W.P., Humes, K.S., 1995. Source approach for estimating soil and vegetation energy fluxes in observations directional radiometric surface temperature. Agric. For. Meteorol. 77, 263–293.
Norman, J.M., Anderson, M.C., Kustas, W.P., French, A.N., Mecikalski, J., Torn, R., Diak, G.R., Schmugge, T.J., Tanner, B.C.W., 2003. Remote sensing of surface energy fluxes at 10^1-m pixel resolution. Water Resour. Res. 39, 1221–1237.
Otkin, J.A., Anderson, M.C., Mecikalski, J.R., Diak, G.R., 2005. Validation of GOES-based insolation estimates using data from the United States Climate Reference Network. J. Hydrometeorol. 6, 460–475.
Ozdogan, M., Gutman, G., 2008. A new methodology to map irrigated areas using multi-temporal MODIS and ancillary data: an application example in the continental US. Remote Sens. Environ. 112, 3520–3537.
Priestley, C.H.B., Taylor, R.J., 1972. On the assessment of surface heat flux and evaporation using large-scale parameters. Mon. Weather Rev. 100, 81–92.
Prueger, J.H., Alfieri, J.G., Hipps, L.E., Kustas, W.P., Chávez, J.L., Evett, S.R., Anderson, M.C., French, A.N., Neale, C.M.U., McKee, L.G., Hatfield, J.L., Howell, T.A., Agam, N., 2012. Patch scale turbulence over dryland and irrigated surfaces in a semi-arid landscape under advective conditions during BEAREX08. Adv. Water Resour. 50, 106–119.
Ross, J., 1975. Radiative transfer in plant communities. In: Monteith, J.L. (Ed.), Vegetation and Atmosphere. Academic Press, London, pp. 13–55.
Santanello Jr., J.A., Friedl, M.A., 2003. Diurnal covariation in soil heat flux and net radiation. J. Appl. Meteorol. 42, 851–862.
Schaible, G.D., Aillery, M.P., 2012. US irrigated agriculture: water management and conservation. In: Osteen, C., Gottlieb, J., Vasavada, U. (Eds.), Agricultural Resources and Environmental Indicators – 2012. EIB-98. US Department of Agriculture, Economic Research Service, Washington, DC, USA, pp. 29–32.
Seguin, B., Becker, F., Phulpin, T., Gu, X.F., Guyot, G., Kerr, Y., King, C., Lagouarde, J.P., Ottlé, C., Stoll, M.P., Tabbagh, A., Vidal, A., 1999. IRSUTE: a multisatellite project for land surface heat flux estimation from field to regional scale. Remote Sens. Environ. 68, 357–369.
Suyker, A.E., Verma, S.B., 1993. Eddy correlation measurements of CO_2 flux using a closed-path sensor: theory and field tests against an open-path sensor. Boundary-Layer Meteorol. 64, 391–407.
Van Niel, T.G., McVicar, T.R., Roderick, M.L., van Dijk, A.I.J.M., Beringer, J., Hutley, L.B., van Gorsel, E., 2012. Upscaling latent heat flux for thermal remote sensing studies: comparison of alternative approaches and correction of bias. J. Hydrol. 468–469, 35–46.
Verma, S.B., Dobermann, A., Cassman, K.G., Walters, D.T., Knops, J.M., Arkebauer, T.J., Suyker, A.E., Burba, G.G., Amos, B., Yang, H.S., Ginting, D., Hubbard, K.G., Gitelson, A.A., Walter-Shea, E.A., 2005. Annual carbon dioxide exchange in irrigated and rainfed maize-based agroecosystems. Agric. For. Meteorol. 131 (1–2), 77–96.
Wan, Z., Li, Z.-L., 1997. A physics-based algorithm for retrieving land-surface emissivity and temperature from EOS/MODIS data. IEEE Trans. Geosci. Remote Sens. 35 (4), 980–996.
Webb, E.K., Pearman, G.I., Leuning, R., 1980. Correction of flux measurements for density effects due to heat and water vapour transfer. Q. J. R. Meteorol. Soc. 106, 85–100.
Wilson, K.B., Baldocchi, D.D., 2000. Seasonal and interannual variability of energy fluxes over a broadleaved temperature deciduous forest in North America. Agric. For. Meteorol. 100, 1–18.